IEEE Access
Multidisciplinary | Rapid Review | Open Access Journal

Received 31 July 2023, accepted 16 August 2023, date of publication 21 August 2023, date of current version 25 August 2023.

Digital Object Identifier 10.1109/ACCESS.2023.3306831

RESEARCH ARTICLE

Voltage Sag Assessment, Detection, and Classification in Distribution Systems Embedded With Fast Charging Stations

SAMI M. ALSHAREEF, (Member, IEEE)
Department of Electrical Engineering, Faculty of Engineering, Jouf University, Sakaka 72388, Saudi Arabia
e-mail: smalshareef@ju.edu.sa

This work was supported by the Deputyship for Research and Innovation, Ministry of Education, Saudi Arabia, under Project 223202.

ABSTRACT A fast charging station (FCS), which consists of eight fast and extreme chargers that operate individually and simultaneously, is considered in this research work. The FCS is supplied from the main grid as well as a Photovoltaic (PV) Farm that includes a two-unit array of 250 kW per array. The impact of the FCS on the voltage sag is quantified using two indices: a voltage sag energy index and a voltage sag severity index. The voltage sag severity is determined based on the sag duration, in accordance with the Semiconductor Equipment and Materials International Group (SEMI) curve. This paper subsequently aims to accurately determine the origin of voltage sag events, whether due to a fault (short circuit) in the system or due to a charging event that occurs at an FCS. The cases in which the voltage sag limit is violated are identified as normal events (due to charging events at the FCS) or anomaly events (due to faults), using a machine learning-based method. Both events of normal and anomaly are simulated based on a Monte Carlo method. Different wavelet functions of different orders are introduced to extract the events' features relying on the change between cycles of the voltage and the current waveform. The minimum redundancy maximum relevance algorithm is applied to obtain an optimal set of features to improve the classification's performance. The results of voltage sag energy index indicate that the voltage sag energy is about 0.28 p.u. for almost 50% of the applied scenarios. Likewise, the sag severity index is more than one for nearly 50% of the charging events considered in this study. Moreover, the findings reveal that all normal and anomaly events are accurately classified using biorthogonal of order 3.9 when ensemble tree or naïve Bayes classifiers are trained and tested by the proposed set of features. Not only can the overall performance of the power system be improved by accurately classifying normal and abnormal events, but power outages are also prevented and maintenance costs are reduced.

INDEX TERMS Fast charging station, voltage sag, electric vehicle, anomaly detection, machine learning.

NOMENCLATURE

ξ_{sag}	The voltage sag energy index.
U_{nom}	The nominal voltage.
U	The retained voltage.
T	The duration of the event.
U_R	The retained voltage of phase R.
U_S	The retained voltage of phase S.
U_T	The retained voltage of phase T.
χ_e	The voltage sag severity index.
U_{curve}	The value of the magnitude of the SEMI F47 reference curve.
φ	The sag event duration.
i	Index of FCS, distribution transformer, or a breaker
T_i	The i^{th} distribution transformer to feed the i^{th} charging station.
S_i	The i^{th} breaker to connect the i^{th} charging station.
$\mathcal{J}$	Index of phase.
$u_{\mathcal{J}}[n]$	The sample value of the voltage signal of the $\mathcal{J}^{th}$ phase.

The associate editor coordinating the review of this manuscript and approving it for publication was Nagesh Prabhu.

$I_{\mathcal{J}}[n]$	The sample value of the current signal of the $\mathcal{J}^{th}$ phase.
n^{th}	Indication of the current instant.
κ	The number of samples per cycle.
$u_{\mathcal{J}}[n-\kappa-1]$	The voltage value sampled one cycle ago.
$i_{\mathcal{J}}[n-\kappa-1]$	The current value sampled one cycle ago.
Ξ_{β}	The energy of the wavelet coefficients of the approximation.
Ξ_{α}	The energy of the wavelet coefficients of the details.
β_j	The wavelet coefficients of the approximation of j^{th} wavelet decomposition level.
α_j	The wavelet coefficients of the detail of j^{th} wavelet decomposition level.
j	Index of wavelet decomposition level.
$\underline{\eta}$	The high pass filters.
$\overline{\eta}$	The low pass filters.
X_r	A given feature ($r \in \{1, 2, \ldots..\omega\}$.
ω	The total number of features.
Ψ	The estimated feature importance.
$I(\Upsilon, \mathrm{X})$	The mutual information for the discrete variables Υ and X.
λ	The class label.
X	A set of the selected feature.
X_s	One feature out of the feature set.
Φ_{Υ}	The sample space of the discrete variable Υ.
Φ_{X}	The sample space of the discrete variable X.
Gini	A measure for selecting the best split.
$\mathscr{g}$	The number of classes.
$p(r\|\vartheta)$	The fraction of records of class r at a given node ϑ.
$\mathcal{S}$	The number of base classifiers.
$\mathcal{C}_i$	The i^{th} base classifier.
$\mathcal{D}$	The original training dataset.
x	A test record.
$\mathcal{C}^*$	Indicator for a majority vote on the individual predictor.
Υ	A random variable.
v	A given class label.
c	A positive value defined by a user indicates to a penalty of misclassifying.
$\mathscr{k}_e$	A slack variable representing the distance from the object that does not lie in the side of its class to the hyperplane.
$\mathcal{A}\mathfrak{cc}$	Index for the accuracy measurement.
$\mathfrak{p}$	Index for the precision measurement.
$\mathfrak{r}$	Index for the recall measurement.
$\mathfrak{T}$	Index for the F-score measurement.
FCS	Fast charging station.
PCC	The point-of-common-coupling.
SEMI	The semiconductor equipment and materials international.
MCS	Monte Carlo simulation.
LUQ	Left upper quadrant.
LLQ	Left lower quadrant.
RUQ	Right upper quadrant.
RLQ	Right lower quadrant.
PV	Photovoltaic.
AF	All feature.
SF	Selected feature.
DWT	Discrete wavelet transform.
TP	True Positive.
TN	True Negatives.
FP	False Positives.
FN	False Negatives.
ODTC	Optimizable decision tree classifier.
SVMC	Support vector machine classifier.
ETC	Ensemble tree classifier.
KNBC	Kernel naïve Bayes classifier.
MRMR	The minimum redundancy maximum relevance.
db	Indication of the Daubechies wavelet function.
bior	Indication of biorthogonal the wavelet function.
coif	Indication of the coiflet wavelet function.
sym	Indication of the symlet wavelet function.

I. INTRODUCTION

A. BACKGROUND

In the modern era, power systems and their customers have become increasingly sensitive to the quality of supplied power due to the heavy reliance of modern industries on power electronic components, smart sensors, and actuators. These devices are highly susceptible to power system disturbances, such as voltage sag which can be considered as the origin of 70 to 90% of power quality problems [1]. Voltage sags, also known as dips, are a momentary reduction in the RMS voltage magnitude in power systems. The critical characteristics of voltage sags are their magnitude and duration, which typically range from 0.1 to 0.9 per unit (p.u.) and 0.5 cycles to 1 minute, respectively [2]. Some equipment, such as personal computers, compact disc players, electronic alarms, video recorders and microwave ovens, can reset due to a short reduction in voltage. Moreover, adjustable-speed drives, or programmable logic controllers for industrial processes, can trip during voltage sags, causing significant economic losses [3]. The voltage sag problem has been addressed in key works published recently and from different aspects aiming to, for instance, estimate its frequency [4], locate its source [5], investigate its impact [6], compensate its impact [7], classify its phenomena [8], [9], and emulate its techniques [8]. Previous work related to voltage sags can be divided broadly into three main groups, the first of which focused mainly on voltage sag assessment [10], [11], [12], [13], [14]

while the second group of studies was devoted to stochastic prediction and/or detection of voltage sags in power systems [15], [16], [17], [18], [19], [20], [21], [22]. The third group of studies estimated the costs of voltage sags and/or the sensitivity of equipment to voltage sags [23], [24], [25], [26], [27], [28], [29]. In order to achieve these aims, the previous studies aimed to investigate the sag magnitude, sag duration, and sag frequency while presuming system faults to be the major cause of voltage sags. Although faults are the main cause of voltage sags at transmission and distribution levels [30], none of the surveyed work has considered the impact of fast charging stations (FCSs) on voltage sags. While monitors can be utilized to obtain an accurate evaluation of voltage sag performance, several dozen years are required to do so [31]. Instead, characteristics of voltage sag can be estimated randomly using a simulation tool.

B. AIM OF THE CURRENT WORK

The goal of the work presented in this paper is to fill the research gap by investigating the impact of fast and extreme charging stations on voltage sags by quantifying both indices of voltage sag energy and voltage sag severity. This paper subsequently aims to accurately determine the origin of voltage sag events, whether due to a fault (short circuit) in the system or to a charging event that occurs at an FCS.

C. CONTRIBUTION

The research presented in this paper is devoted to estimating the effect of operating different extreme fast chargers, whether individually or simultaneously, on the power distribution system's voltage sag. The key contributions of this work are summarized as follows:

1. Quantifying the impact of FCSs on voltage sag using two indices, as recommended by IEEE standard: voltage sag energy index and voltage sag severity index.
2. Applying the minimum redundancy maximum relevance algorithm to obtain an optimal set of features that can be utilized to improve detection and classification performance.
3. Proposing a wavelet function of a specific order and a machine learning classifier, applied to the change between cycles of the voltage and current signals, in order to obtain the best classification accuracy.
4. Detection and classification of the origins of voltage sag, whether based on normal events (charging) occurring at FCSs or based on anomaly events (faults) occurring in the distribution power system.

II. PROBABILISTIC ASSESSMENT OF VOLTAGE SAG

A. FAST CHARGING STATIONS

A voltage sag is a transient event caused by various reasons such as motor starting and sudden load changes. An FSC requires high power from the electric grid, varying from zero (when the FCS is ideal) to the maximum rated power of the charger (when the FCS is occupied), and then charging that power over a period of time into electric vehicles (EVs). Therefore, the operation of an FCS depicts the pattern of both motor starting (by requiring a high current from the grid) and sudden load changes (by changing between the two states of idle and occupied). When a station consists of more than one charger, the amount of power required from the grid, as well as the changes between the two states, are increased and thus may lead to a voltage sag.

B. VOLTAGE SAG INDICES

A sag in the electric power system voltage is characterized by two attributes: the lowest root-mean-square (rms) voltage during the event, known as the retained voltage, and the time that the retained voltage stays below a predefined limit, which is termed a sag duration. The IEEE Guide for Voltage Sag Indices (IEEE Std 1564-2014 [32]) gives the recommended value for the sag threshold as 90% of the nominal voltage and, accordingly, the sag duration is the amount of time (number of cycles) the rms stays below 90% of the declared voltage. In this work, two indices that are recommended in [32], namely the voltage sag energy index and the voltage sag severity index, are utilized to quantify the impact on voltage sag of an FCS

Voltage sag energy index:the voltage sag energy, ξ_{sag}, is defined as:

$$\xi_{sag} = \int_0^T \left[1 - \left(\frac{U(t)}{U_{nom}}\right)^2\right] dt \tag{1}$$

where $U(t)$ is the rms voltage value calculated over the duration of the event and U_{nom} is the nominal voltage. Furthermore, when the rms voltage is assumed to be constant during the event, the voltage sag energy is determined as:

$$\xi_{sag} = \left[1 - \left(\frac{U}{U_{nom}}\right)^2\right] \times T \tag{2}$$

where U and T are the retained voltage and the duration of the event, respectively. For the case of a three-phase sag, the retained voltage of each phase is utilized to calculate the voltage sag energy as:

$$\xi_{sag} = \left[3 - \left[\left(\frac{U_R}{U_{nom}}\right)^2 + \left(\frac{U_S}{U_{nom}}\right)^2 + \left(\frac{U_T}{U_{nom}}\right)^2\right]\right] \times T \tag{3}$$

where U_R, U_S, and U_T are, respectively, the retained voltage of phase R, S, and T.

Voltage sag severity index: In order to calculate the voltage sag severity index, the IEEE Guide for Voltage Sag Indices recommends using the Semiconductor Equipment and Materials International Group (SEMI) F47 curve [33] as well as the per unit retained voltage and duration of the voltage sag. The voltage sag severity index, χ_e, is defined as:

$$\chi_e = \frac{1 - U}{1 - U_{curve}(\varphi)} \tag{4}$$

TABLE 1. Algorithm for estimating the severity of voltage sag.

Period of sag event	Estimated value of sag severity
$\varphi \leq \frac{f}{50}$	$\chi_e = 1 - U$
$\frac{f}{50} < \varphi \leq \frac{f}{5}$	$\chi_e = 2(1 - U)$
$\frac{f}{5} < \varphi \leq \frac{f}{2}$	$\chi_e = 3.3(1 - U)$
$\frac{f}{2} < \varphi \leq 10.f$	$\chi_e = 5(1 - U)$
$\varphi > 10.f$	$\chi_e = 10(1 - U)$

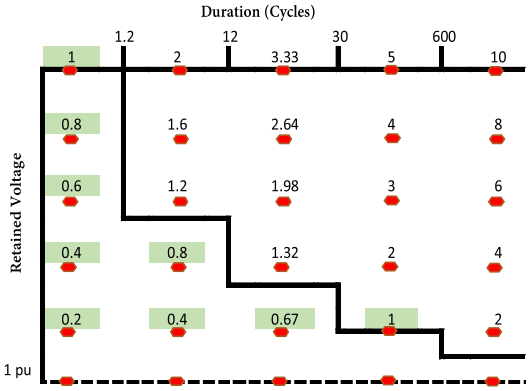

FIGURE 1. Severity of voltage sag based on the SEMI F47 curve.

where $U_{curve}(\varphi)$ is the value of the magnitude of the reference curve corresponding to the event duration φ.

The idea of the SEMI curve is outlined in Fig. 1. Given both the depth of a voltage sag and its duration, χ_e is calculated according to its position on the reference in Fig. 1. For an event on the reference curve, χ_e is equal to one. For an event below the reference curve, χ_e is less than one, and for an event above the reference curve, χ_e is more than one. Table 1 can be utilized to determine the voltage sag severity as per the SEMI curve.

III. INPUT DATA REQUIRED FOR VEHICLE CHARGING MODEL

A. BACKGROUND

In general, disturbance classification consists of three steps: 1. signal analysis and feature extraction; 2. feature selection; and 3. disturbances classification [34]. For signal analysis, several approaches have been developed based on signal processing techniques. These include fast Fourier transform (FFT); discrete Fourier transforms (DFT); short-time Fourier transform (STFT); S-transform (ST); and wavelet transform (WT) [35]. The signal processing technique is selected based on the nature of the signal under study. The WT decomposes the signal into several levels, while features such as wavelet coefficients, energy, and entropy are extracted [36]. The feature extraction process is usually excessively arbitrary. Following the signal decomposition and feature extraction stages, the feature selection is conducted. If the number of features is high, the best features are selected, but why the previous work chose these features, and whether they are conducive to discriminating different power quality disturbances (i.e., voltage sag), has yet to be clearly answered. In order to solve this problem, researchers have paid attention to filtrating features through an optimization algorithm so as to capture the most critical features for power quality disturbance classification. In [37], the artificial bee colony method is used for the optimal feature selection of power quality disturbances. A particle swarm optimization method is employed in [38] to find the optimal number of input features. In [39], an adaptive probabilistic neural network is used as a global optimization algorithm to gradually remove redundant and irrelevant features in noisy environments. Subsequently, classifiers are used to classify power quality disturbances. For this purpose, in the literature, different classifiers are used, such as artificial neural networks (ANN) [40], support vector machines (SVMs) [41], decision trees (DTs) [42], and deep learning techniques [43].

B. RESEARCH METHODOLOGY

A layout of the proposed methodology is depicted in Fig. 2. The methodology for this paper involves the following steps:

1. Data collection: the IEEE 4 bus test system is utilized to conduct different case studies and generate the data. The collected data are the three phase voltage and current signals measured at the bus in which the FCSs are integrated.
2. Classification of voltage sag events: voltage sag events are classified into two events, namely normal and anomaly. Normal events are caused by charging events at FCSs while anomaly events are caused by faults at the power grid.
3. Feature extraction and selection: discrete wavelet transform (DWT) is utilized to extract features of the collected data. The best features are then selected according to defined criteria that are illustrated in Section III-E. These features will be used as inputs to the anomaly detection model.
4. Normal and anomaly detection model: after the features are extracted and selected, a machine learning technique is utilized for anomaly detection. The model's performance can be evaluated using different indices, such as accuracy, precision, and recall.

C. DISTRIBUTION SYSTEM DESCRIPTION

The work presented in this paper considers the IEEE 4 bus test system that operates at a nominal voltage of 12.47 kV [44]. A one three-phase transformer bank is utilized to step down the system voltage from 12.47 kV to 4.16 kV in order to meet the demand of a delta connected load, at a distance of 1.372 km away from the substation, at bus 4. The rated capacity of the transformer is 6000 kVA where the spot load of each line-to-line is rated as 1.5 MVA, 2 MVA, and 2.5 MVA,

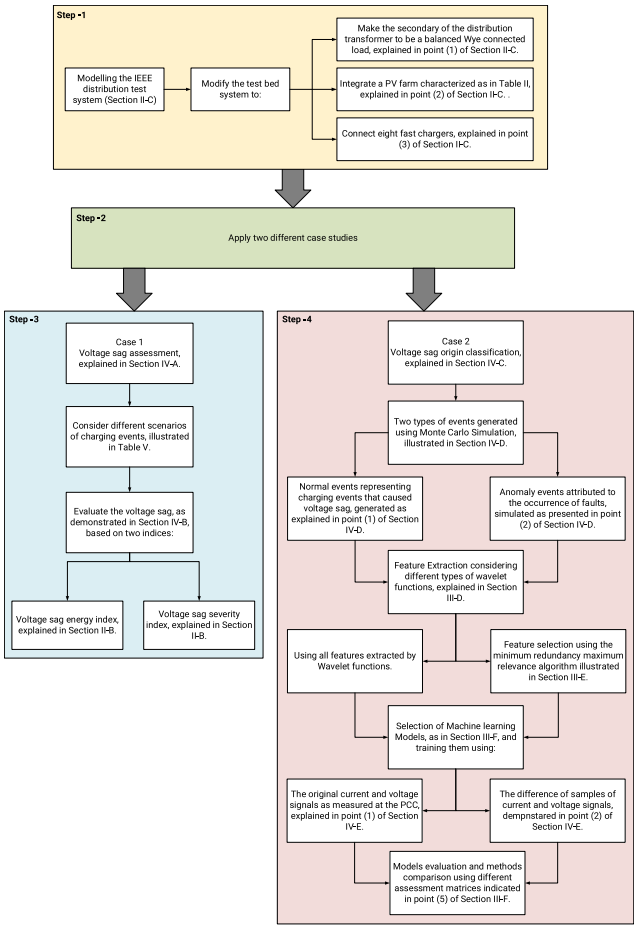

FIGURE 2. Flowchart of the proposed methodology.

at 0.85, 0.9, and 0.95 lagging power factor, respectively. More details of the operating conditions of the distribution system under study can be found in [45].

1) DISTRIBUTION SYSTEM MODIFICATION

The configuration of load at bus 4 of the distribution system under study is modified to be a balanced Wye connected load rated as 1.5567 MW and 0.8143 MVar per phase and thus the secondary of the distribution transformer is also modified to Wye connection. Furthermore, the PV farm and FCSs are integrated into the test system, as depicted in Fig. 3.

2) PV FARM'S INTEGRATION

A two-unit PV array of 250 kW per PV array is connected to the test system, at the system's utilization voltage level, via a three-phase transformer rated 5000 kVA, as indicated in Fig. 3. The solar farm mainly consists of a power plant controller, a PV array, a boost converter, and a DC-AC inverter [46]. The power plant controller is used primarily for adjustment of the reference powers (i.e., active, reactive) of the inverter in the solar farm according to the measured values of voltage, active, and reactive powers at the point-of-common-coupling (PCC). Each PV array generates a maximum power of 250 kW at the nominal temperature and irradiation of 28℃ and $1000W/m^2$, respectively. The boost converter is utilized to obtain the maximum power point tracking via control of the DC voltage. The dynamic of the solar farm is controlled using the DC-AC inverter. Characteristics of the PV system are shown in Table 2.

3) FAST CHARGING STATIONS' CONNECTION

There are eight FCSs connected to the distribution test system at the PCC. Each FCS is connected to the system via a distribution transformer (T_i) which is connected to FCS_i via S_i breaker, where i indicates the FCS number. Here, the output power of FCS_1, FCS_2, FCS_3, and FCS_4 is equal to the output power of FCS_5, FCS_6, FCS_7, and FCS_8, respectively. Thus, the rated kVA of the transformer T_1, T_2, T_3, and T_4 is equal to the kVA rated of T_5, T_6, T_7, and T_8. Each distribution transformer T_i steps down the primary voltage of 4.16 kV to 0.480 kV, the voltage level utilized by each FCS_i. Each breaker S_i has two states, namely on and off. The state "on" indicates that the breaker S_i is closed, hence the FCS_i is occupied. The state "off" means that the breaker S_i is open and thus FCS_i is idle. Although the current that passes via two different breakers may be equal, the states of each breaker S_i is independent of the other breaker's states.

D. WAVELET-BASED DATASET COLLECTION

For each simulated event (normal or anomaly) that causes a voltage sag, the voltage and current samples of the three-phases at the PCC, to which the PV farm is tied, are utilized to create the attributes matrix. The attribute matrix includes the transient signature of the sampled current and voltage. Two methods are utilized to build the attribute matrix in order to include: 1) the transient signature of the sampled current and voltage as measured at the PCC; and 2) the difference between two samples one cycle apart [47], as in equations (5) and (6). In each method, the attribute matrix consists of κ number of samples where κ is the number of samples per cycle.

$$U_{\mathcal{J}}[n] = u_{\mathcal{J}}[n] - u_{\mathcal{J}}[n-\kappa-1] \tag{5}$$

$$I_{\mathcal{J}}[n] = i_{\mathcal{J}}[n] - i_{\mathcal{J}}[n-\kappa-1] \tag{6}$$

where $\mathcal{J}$ is an index for each phase (i.e., R, S, and T), $u_{\mathcal{J}}[n]$ and $I_{\mathcal{J}}[n]$ represent, respectively, the sample values of the voltage and current signals of the $\mathcal{J}^{th}$ phase, at the n^{th} instant, $u_{\mathcal{J}}[n-\kappa-1]$ and $i_{\mathcal{J}}[n-\kappa-1]$ are the voltage and current values sampled one cycle ago, (i.e., before $\approx 0.01667\ s$), and $U_{\mathcal{J}}[n]$ and $I_{\mathcal{J}}[n]$ are the values included in the attribute matrix as per the second method. The DWT is applied to decompose the attribute matrix to the wavelet space in order to extract the hidden features of the sampled data. The decomposition level is determined based on the sampling rate of the three-phase sampled signals. The three-phase voltage and current signals that are sampled at κ (i.e., $\kappa = 256$) samples per cycle results in a sampling rate of 15.36 kHz. Therefore, six decomposition levels are

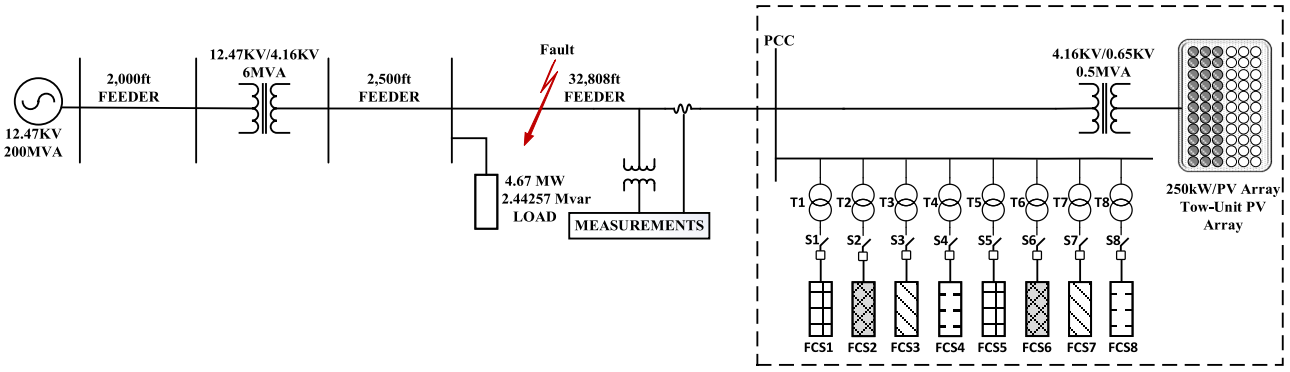

FIGURE 3. Single line diagram of the modified IEEE 4 bus test feeder.

required to center the power system frequency (60 Hz) in the lowest band of the original signal (scaling level j_o) as well as for extracting the features in all wavelet sub-bands. Among many sets of wavelet basis functions, four wavelet families (Daubechies (db#), Biorthogonal (bior#), Coiflet (coif#), and Symlet (sym#)) at different orders, as presented in Table 3, are used for extraction features of the sampled signals, selected according to their characteristics as well as for their superior performance in the previous work that studied voltage quality (i.e., sag) [48], [49], [50], [51]. Here, the # symbol indicates the order of that given wavelet function. In this paper, the energy of the wavelet coefficients of the approximation Ξ_β and of the details Ξ_α are utilized as indices for classifying the origin of voltage sag. In order to obtain the energy of the wavelet coefficients, the wavelet coefficients of the approximation (β_j) and detail (α_j) of each wavelet decomposition level j are calculated as follows:

$$\beta_j(k) = \sum_n \underline{\eta}(n-2k)\beta_{j-1}(n) \tag{7}$$

$$\alpha_j(k) = \sum_n \overline{\eta}(n-2k)\alpha_{j-1}(n) \tag{8}$$

$$\Xi_{\beta j} = \sum_n \left|\beta_j(k)\right|^2 \tag{9}$$

$$\Xi_{\alpha j} = \sum_n \left|\alpha_j(k)\right|^2 \tag{10}$$

where $\underline{\eta}$ and $\overline{\eta}$ are the low pass and high pass filters, respectively.

E. FEATURE SELECTION

For each phase of the three-phase voltage and current signals, the energy of the wavelet coefficients is calculated at all levels of wavelet decomposition (six levels). As a result, seven attributes are extracted for each phase (six detailed wavelet decompositions and one approximation). Therefore, the feature matrix, whether for normal or anomaly events, consists of 42 attributes in columns (seven per phase for current and voltage signals), but 128 and 132 records in rows for normal and anomaly events, respectively. To reduce the number of attributes and obtain an optimal set of features,

TABLE 2. Specification of the PV system.

Input parameters of PV array	Value
Number of modules connected in series per array	35
Number of modules strings in parallel per array	130
Number of cells connected in series per module	35
Number of cell strings in parallel per module	1
Reference irradiation, Γ_r	1000
Reference cell temperature, γ_r	28
Short circuit current at reference conditions per cell	0.0025 kA
Open circuit voltage at reference conditions per cell	0.000843 kV
Current at maximum power point	0.300 kA
Voltage at maximum power point	0.833 kV

the minimum redundancy maximum relevance (MRMR) algorithm is applied with the aim of minimizing the redundancy and maximizing the relevance of a feature set to the response variable [52]. Let ω represent the total number of features (i.e., 42), and X_r is a given feature ($r \in \{1, 2, \ldots..\omega\}$), then the estimated feature importance by the MRMR, based on the mutual information quotient, is defined as:

$$\Psi_{MRMR}(\chi_r) = \frac{I(\Upsilon, \mathrm{X}_r)}{\frac{1}{|\lambda|}\sum_{\chi_s \in \lambda} I(\mathrm{X}, \mathrm{X}_r)} \tag{11}$$

where Υ, λ, and $|\lambda|$ are the class label, a set of the selected feature, and the size of feature set, $\mathrm{X}_s \in \lambda$, is one feature out of the feature set λ, $\mathrm{X}_r(\mathrm{X}_r \notin \lambda)$ is a feature currently not selected, and $I(.,.)$ denotes the mutual information and is calculated for discrete variables Υ, X as follows:

$$I(\Upsilon, \mathrm{X}) = \sum_{\upsilon \in \Phi_\Upsilon, \chi \in \Phi_\mathrm{X}} P(X = \chi, \Upsilon = \upsilon) \times \log \frac{P(X = \chi, \Upsilon = \upsilon)}{P(X = \chi)\, P(\Upsilon = \upsilon)} \tag{12}$$

where Φ_Υ and Φ_X are the sample spaces of Υ and X, respectively. If X and Υ are independent, then the mutual information (I) equals 0. However, if X and Υ are similar variables, then the mutual information (I) equals the entropy

TABLE 3. Comparison of different wavelet functions based on defined criteria.

Ref.	Wavelet function	Filter length	Vanishing moments	Compact support width	Orthogonality	Near symmetric/ symmetric*	Biorthogonality
[46]	db3	6	3	5	✓	×	✓
[43]	db4	8	4	7	✓	×	✓
[47]	db6	12	6	11	✓	×	✓
[44]	db8	16	8	15	✓	×	✓
[48]	db10	20	10	10	✓	×	✓
[49]	coif3	18	6	17	✓	✓	✓
[49]	coif5	30	10	29	✓	✓	✓
[50]	sym4	8	4	7	✓	✓	✓
[51]	sym8	16	8	15	✓	✓	✓
[52]	sym10	20	10	19	✓	✓	✓
[53]	bior2.2	6	2 and 2	5	×	✓*	✓
In this work	bior3.9	20	3 and 9	19	×	✓*	✓

of X. The feature that has the largest value of Ψ_{MRMR} with nonzero redundancy and nonzero relevance in $\lambda^{\mathbb{C}}$, the complement of λ, is selected. If the given rank score by the MRMR is large, this indicates that the corresponding feature is important. As the variation of the feature importance score is increased, the confidence of that selection is also increased.

F. MACHINE LEARNING ALGORITHM

1) OPTIMIZABLE DECISION TREE CLASSIFIER

The first classifier considered in this paper is an optimizable decision tree classifier (ODTC). Unlike traditional decision trees that use a fixed set of decision rules, an ODTC is able to learn and optimize the decision rules during the training process. The main idea behind an ODTC is to represent the data as a tree-like structure, where each node represents a decision rule that splits the data whereby the best splits are selected based on the minimum degree of impurity measured by the Gini index as [53]:

$$Gini\,(\vartheta) = 1 - \sum_{r=0}^{\mathscr{g}-1} |(p(r|\vartheta)|^2 \tag{13}$$

where $\mathscr{g}$ indicates the number of classes and $(p(r|\vartheta)$ represents the fraction of records of class r at a given node ϑ. The goal is to find the decision rules that best separate the normal (FCS events) and anomaly classes (faults' events). During the training process, the algorithm iteratively splits the data into smaller and smaller groups until each group contains only events of the same class. This process results in a decision tree that can be used to classify new events as normal or anomaly. The ODTC can optimize the decision rules by using a loss function, which measures the performance of the tree on the training data. The algorithm adjusts the decision rules to minimize the loss function, leading to improved accuracy in classifying new events. The loss function can be chosen to reflect the nature of the problem and the desired accuracy. Some common loss functions include the mean squared error and the cross-entropy loss.

2) ENSEMBLE TREE CLASSIFIER

The main objective of training models using ensemble methods is for improving classification accuracy by aggregating the predictions of multiple classifiers. The ensemble tree classifier (ETC) technique "constructs a set of base classifiers from training data and performs classification by taking a vote on the prediction made by each base classifier" [53]. The general procedure to build the ensemble tree is as follows: create a training set from the original data $\mathcal{D}$. Subsequently, from each training set $\mathcal{D}_i$, construct a base classifier $\mathcal{C}_i$, then, according to the majority vote of the base classifiers $\mathcal{C}_i$, a test record x is classified as:

$$\mathcal{C}^*(x) = Vote(\mathcal{C}_1\,(x)\,, \mathcal{C}_2\,(x)\,, \ldots\ldots\ldots, \mathcal{C}_{\mathcal{S}}\,(x)) \tag{14}$$

where $\mathcal{S}$ is the number of base classifiers. In this study, the technique utilized for constructing the ensemble decision tree is "bootstrap aggregation", known as "bagging". This technique works by taking a base learning classifier and recalling it many times using different training sets [54], whereby samples of the training data can be replaced during the training stage to improve the model's performance.

3) KERNAL Naïve BAYES CLASSIFIER

The naïve Bayes (NB) classifier works on the assumption that the independence of attributes given a class label v is determined as follows [55]:

$$P\,(\mathrm{X}|\Upsilon = v) = \prod_{r=1}^{\omega} P(\mathrm{X}_r|\Upsilon = v) \tag{15}$$

where each features set $\mathrm{X} = \{\mathrm{X}_1, \mathrm{X}_2, \ldots\ldots\ldots, \mathrm{X}_\omega\}$ consists of ω attributes. In order to classify a test record x by the NB classifier, it is necessary to determine the posterior probability for each class v as follows:

$$P\,(\Upsilon = v|\mathrm{X}) = \frac{P(\Upsilon)\prod_{r=1}^{\omega} P(\mathrm{X}_r|\Upsilon = v)}{P(\mathrm{X})} \tag{16}$$

Thus, the class that maximizes the value of the numerator is selected since the value of $P(\mathrm{X})$ is fixed for each class Υ. The main concept behind the kernel naïve Bayes classifier (KNBC) is to map the data into a high-dimensional

TABLE 4. Confusion matrix for two classes.

		Actual Class: Positive	Actual Class: Negative
Predicted class	Positive	True Positive (TP)	False Positive (FP)
	Negative	False Negative (FN)	True Negative (TN)

feature space, where the data can be more easily separated into classes. The algorithm achieves this by using a kernel function, which transforms the original features into a new set. The kernel function can be chosen to reflect the nature of the data and the problem being solved. Some common kernel functions include radial basis functions, polynomial functions, and sigmoid functions. Once the data has been mapped onto the high-dimensional feature space, the naïve Bayes algorithm is applied to classify the data into normal or anomaly classes. The algorithm works by estimating the probability distribution of each class and then using Bayes' theorem to calculate the probability that a new event belongs to each class. The class with the highest probability is then assigned to the new event [55].

4) SUPPORT VECTOR MACHINE CLASSIFIER

A support vector machine classifier (SVMC) constructs a decision boundary that can separate the training examples and classify them into their corresponding classes. The decision boundary may be linear or nonlinear, as is the case in most real-world problems. Therefore, due to the difficulty of linearly separating the training examples in their input space, a transformation is required to map the training examples from their input space into a higher-dimensional space, where they can be linearly separated. The learning task of this non-linear classifier of the SVM can be seen as an optimization problem [56]:

$$\min_{w,b,k} \frac{1}{2} w^T w + c \sum_{e=1}^{j} \hbar_e \tag{17}$$

$$\mathcal{Y}_e \left(w^T \phi \left(\mathcal{S}_e \right) + b \right) \geq 1 + \hbar_e \tag{18}$$

$$\hbar_e \geq 0 \tag{19}$$

where c and $\hbar_e$ are positive values that can be defined by a user and $\mathcal{Y} \in \{1, -1\}^j$. c indicates the penalty of misclassifying the training examples, and $\hbar_e$ is a slack variable representing the distance from the object that does not lie in the side of its class to the hyperplane. The Gaussian kernel function, as defined in (4), which is utilized in this paper, satisfies the so-called Mercer's conditions [56].

5) ASSESSMENT MATRICS

The purpose of testing the models on unseen data is to investigate their level of accuracy. Accuracy for models is computed as the ratio of the number of records that classified accurately with the total number of records. The confusion matrix is a tool in machine learning that is commonly used to assess the performance of a classifier. It is a table that summarizes the correct and incorrect predictions made by the classifier for different categories. The confusion matrix provides valuable information about the performance of the classifier and helps to identify areas for improvement. Table 2 shows the confusion matrix of two variables. Accuracy for models is computed based on the confusion matrix as the ratio of the numbers of instances that classified accurately with the total number of instances.

$$Accuracy,\ \mathcal{A}\mathfrak{cc} = \frac{TP + TN}{TP + FP + FN + TN} \times 100 \tag{20}$$

Moreover, precision and recall are two metrics that are calculated from the confusion matrix to evaluate the performance of the classifier. It may be noted from Table 4 that there are four parameters. A brief description of each parameter is provided below:

True Positives (TP): These are the correct positive predictions made by the classifier representing the number of anomaly events that are correctly classified.

False Positives (FP): These are incorrect positive predictions made by the classifier indicating to the number of anomaly cases that are misclassified as normal events.

False Negatives (FN): These are incorrect negative predictions made by the classifier; thus this indicates the number of normal events that are misclassified as anomaly events.

True Negatives (TN): These are the correct negative predictions made by the classifier, thus representing the number of normal events that are correctly classified.

Hence, precision and recall are calculated, respectively, as:

$$Precision,\ \mathfrak{p} = \frac{TP}{TP + FP} \tag{21}$$

$$Recall,\ \mathfrak{r} = \frac{TP}{TP + FN} \tag{22}$$

The F-measure ($\mathfrak{T}$) is determined as in (23) to estimate the extent to which a group includes only instances of a particular class and all instances of that class [57]:

$$\mathrm{F-measure}, \mathfrak{T} = \frac{2 \times \mathfrak{p} \times \mathfrak{r}}{\mathfrak{p} + \mathfrak{r}} \tag{23}$$

IV. EVALUATION AND RESULTS

A. CASE 1: VOLTAGE SAG ASSESSMENT

In this case, the impact of FCSs on voltage sag is investigated, using the test bed system shown in Fig. 3. Different scenarios are applied where these scenarios rely on the breakers' states. As an example, in each applied scenario, one breaker, S_i, will be turned on at time t, to activate the FCS_i, while the other breakers will have been turned on and/or off in advance. Thus, in each scenario, an FCS, controlled by the breaker of interest, is activated and consequently draws a large current from the grid to meet the rated power of that FCS (similar to starting a motor). The number of scenarios generated for each

TABLE 5. Switching strategy proposed to consider different cases according to the activated fast charger.

Case number		Breakers															
		S1		S2		S3		S4		S5		S6		S7		S8	
01-128	S1	On at t sec		On	Off	On	Off	On	Off	On	Off	On	Off	On	Off	On	Off
129-256	S2	On	Off	On at t sec		On	Off	On	Off	On	Off	On	Off	On	Off	On	Off
257-384	S3	On	Off	On	Off	On at t sec		On	Off	On	Off	On	Off	On	Off	On	Off
385-512	S4	On	Off	On	Off	On	Off	On at t sec		On	Off	On	Off	On	Off	On	Off
513-640	S5	On	Off	On	Off	On	Off	On	Off	Off at t sec		On	Off	On	Off	On	Off
641-768	S6	On	Off	On	Off	On	Off	On	Off	On	Off	Off at t sec		On	Off	On	Off
769-896	S7	On	Off	On	Off	On	Off	On	Off	On	Off	On	Off	Off at t sec		On	Off
897-1024	S8	On	Off	On	Off	On	Off	On	Off	On	Off	On	Off	On	Off	Off at t sec	

breaker of interest is determined by 2^{n-1}, where the numbers 2 and n represent states of the breaker and the number of breakers in the test system controlling the FCSs. Switching any breaker on or off means switching on or off the FCS that is controlled by that breaker (similar to sudden load changes). When breakers S_1, S_3, and S_4 are closed, the current passing through breaker S_1 is equal to one-third or one-fifth of the current that passes through breakers S_3 and S_4, respectively. When all breakers, shown in Fig. 3, are closed, the active power required by FCSs at the PCC is equal to 1.28 MW fulfilled by the main grid as well as the PV farm. The simulated cases (1024 cases) considered for this case study are listed in Table 5. In each simulated case, one of the eight breakers is closed at time t ($at\ t = 1.5\ s$), indicating that one of the FCSs, to which the breaker is connected, is occupied at that instance of time while the rest of the breakers are either switched on and/or off before that time t. The reason for simulating the large number of cases is to assess the impact of FCSs on the voltage sag under all the possible scenarios.

B. EVALUATION OF CASE 1

In this section, the impact of the FCS on the voltage sag is quantified using two indices: the voltage sag energy index, ξ_{sag}, and the voltage sag severity index, χ_e. The rms voltage value, at the PCC, is compared with the voltage sag threshold. When a charging event at any of the fast chargers (depicted in Fig. 3) causes the rms voltage at the PCC to remain below 90% of its nominal voltage value for a number of cycles (shown in Table 1), that charging event considers the voltage sag scenario. For example. Fig. 4 depicts the rms current and voltage waveforms calculated for the three-phase. In Fig. 4, the breaker S_3 is switched ON at time t (labelled as (2) in the figure) indicating that a charging event is occurring at FCS_3, while S_2 was switched ON in advance indicating

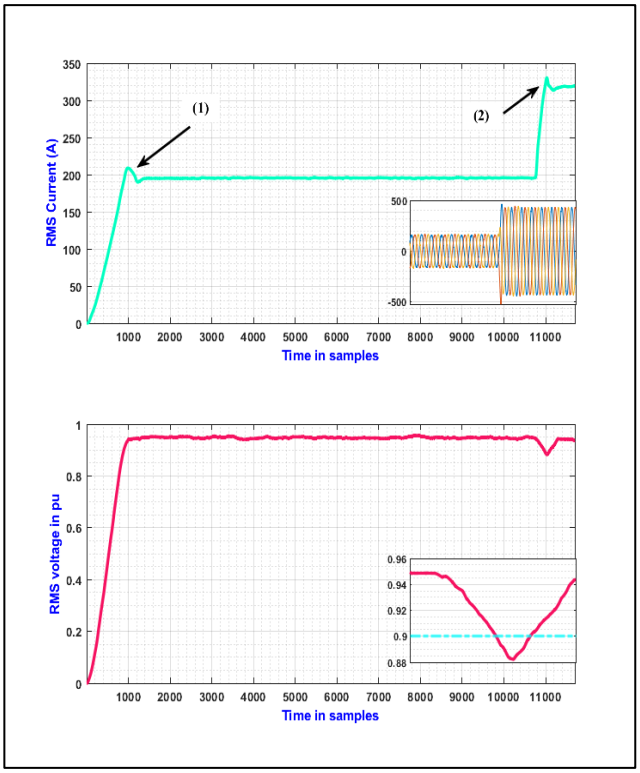

FIGURE 4. Current (top) and voltage (bottom) waveforms measured at PCC when FCS_2 and FCS_3 are occupied.

that a charging event is occurring at FCS_2 (labelled as (1) in Fig 4. When breaker S_3 was switched ON, the drawn current at the PCC was increased making the voltage to dip below the threshold, as shown in the bottom plot of Fig. 4. Each point in Fig. 5(a) can be projected onto the horizontal and vertical axes which represent, respectively, the maximum

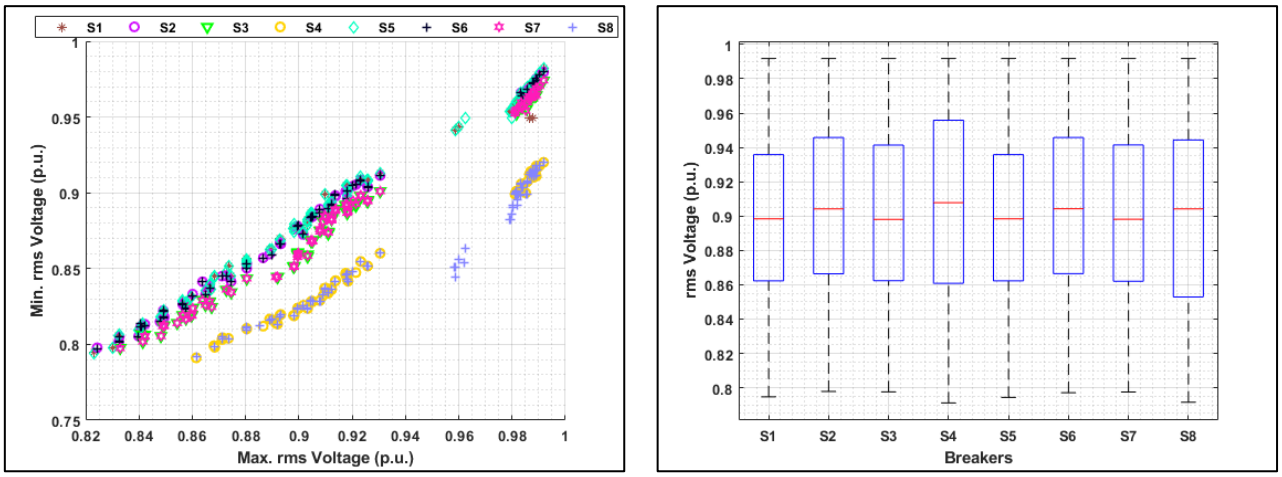

FIGURE 5. Extreme values of rms voltage during different charging events. (a) Minimum and maximum rms voltage per charging event of each breaker. (b) Box plot of rms voltage per breaker utilized to activate a fast charger.

and minimum rms voltages for a charging event occurring at FCS_i, when one breaker, S_i, was turned on at time $t = 1.5\ s$, while the other breakers were turned on and/or off in advance. The overlap of the rms voltage is depicted in Fig. 5(a), for charging events occurring at different slots (i.e., FCS_4 and FCS_8) due to the equality of their output, as mentioned in point (3) of Section III-C. Moreover, Fig. 5(b) displays the boxplot that summarizes the rms voltage of all charging events that occurred at each fast chargerFCS_i, using the values of maximum, minimum, median, and the first and third quartiles. Fig. 6(a) depicts the frequency of occurrence of the minimum rms voltage measured at the PCC for all charging scenarios considered in this case study that violated the limit of voltage sag. Given the sag duration, the cumulative probability is presented on the right side of the y-axis in Fig. 6(a), demonstrating that the minimum rms voltage value is 0.85 p.u. for about 50% of the applied scenarios in this case study. Furthermore, frequency of occurrence of the voltage sag energy, as well as its cumulative probability, is shown in Fig. 6(b), indicating that the voltage sag energy, or interpreted as lack of energy not delivered to an impedance load, is about 0.28 p.u. for almost 50% of the applied scenarios. The results of voltage sag severity index are presented in the x-axis of Fig. 7(a). The voltage sag severity is determined based on the sag duration, in accordance with the SEMI curve shown in Fig. 1. If the magnitude of any charging event is below the voltage sag threshold (90%), the result of the event is included in Fig. 7. When the voltage sag severity index, depicted in Fig. 7, is more than one, it means that the magnitude of that event, from which the voltage sag severity was calculated, is below the SEMI curve shown in Fig. 1. In contrast, a voltage sag severity index of less than one indicates that the magnitude of that event is above the SEMI curve. The sag severity index is more than one for nearly 50% of the charging events considered in this case study, as shown on the right side of the y-axis, in Fig. 7(a). Furthermore, Fig. 7(b) presents the frequency of occurrence of the voltage sag severity of all charging events that occurred at each fast charger FCS_i. The frequency of occurrence among all charging events that occurred at the fast charger FCS_4 result in the highest frequency of occurrence for a voltage sag severity of more than 1.3, as presented in Fig. 7(b).

C. CASE 2: VOLTAGE SAG ORIGIN CLASSIFICATION

In this case study, two different scenarios are considered. Faults at the modified distribution test system, shown in Fig. 3, are applied to generate the data for the first scenario whereas FCSs are integrated into the test system to generate the data for the second scenario. Both of these two scenarios may lead to a temporary reduction in voltage at the PCC, which is known as a voltage sag. The aim of this case study is to distinguish between the origins of the voltage sag in order to determine whether it is attributed to the occurrence of faults at the distribution system or the activation of an FCS.

1) NORMAL EVENTS

When any breaker S_i, shown in Fig. 3, is closed, the FCS_i controlled by that breaker is activated (switched on), indicating that a charging event is occurring at that instance of time. Upon switching states of the breakers, different FCSs are activated/disactivated, indicating that FCSs are occupied/idle at the time of switching the breakers. The time of switching the breakers for all events generated in this case are the same ($at\ t = 1.5\ s$). The rms voltage at the PCC is monitored and compared with the level of voltage sag. The cases where the voltage sag limit are violated are utilized for further processing and labeled as normal events. Although these cases caused voltage sags, they are the result of charging events that occurred at FCSs and thus are identified as normal events.

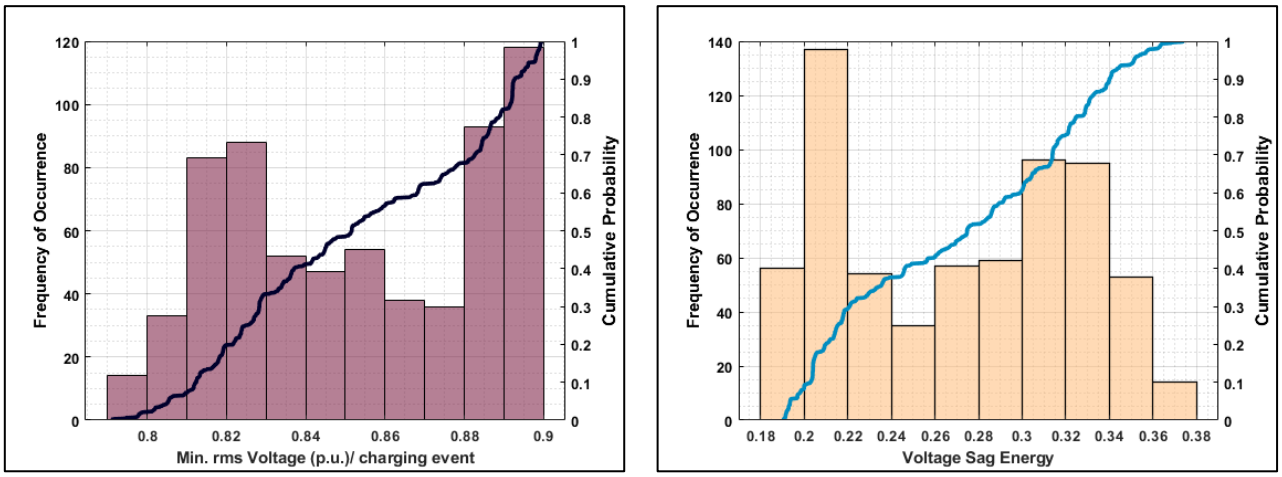

FIGURE 6. Frequency of occurrence and cumulative distribution function. (a) Minimum rms voltage per charging event. (b) Voltage sag energy.

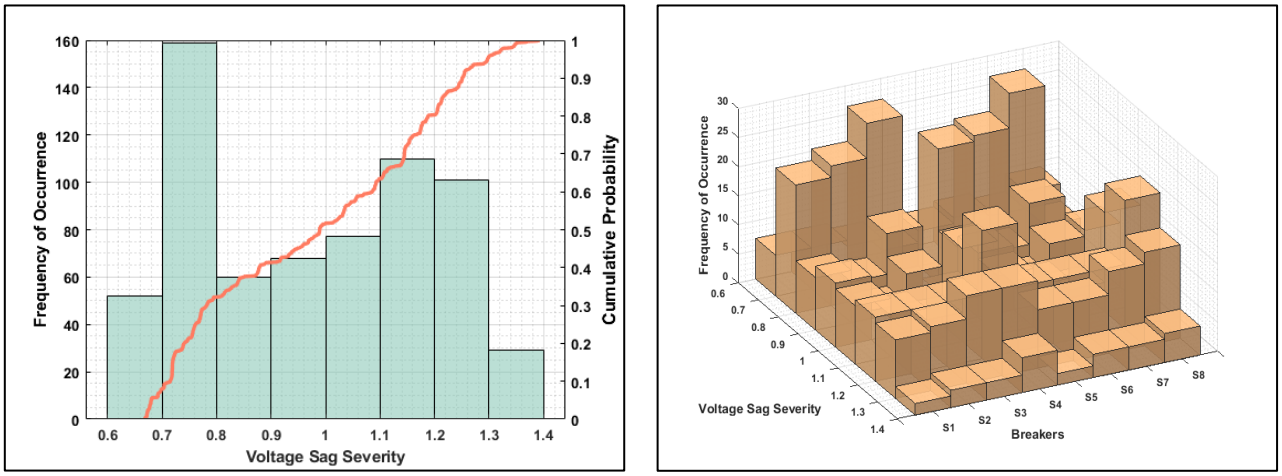

FIGURE 7. Frequency of occurrence and cumulative distribution function. (a) Voltage sag severity. (b) Voltage sag severity per breaker.

2) ANOMALY EVENTS

Most voltage sags in a distribution system are attributed to the occurrence of faults. Thus, different types of ground and non-ground faults, such as three-phase, two-phase, and single-phase, are simulated at 16,404 ft away from the PCC, as shown in Fig. 3. Various values of fault resistance, such as 0.001 Ω, 0.01 Ω, 0.1 Ω, 1 Ω, 10 Ω, and 100 Ω, are considered for each type of simulated fault. The time of applying each type of fault in this scenario is the same ($at\ t = 1.5\ s$) and lasts for the same duration (four cycles). Cases where the rms voltage at the PCC violates the level of the voltage sag are labeled as anomaly events.

D. EVENETS GENERATED IN MONTE CARLO SIMULATION

The cases of both normal and anomaly events are generated based on a Monte Carlo simulation (MCS). Variables of each event are generated randomly based on a uniform distribution.

1) SEMULATED NORMAL EVENTS

Variables that are randomly generated for normal events are breakers' states (i.e., S1, S2, etc.) PV irradiation, and PV cell temperature. Referring to Table 5, breakers' states are divided into four quadrants: left upper quadrant (LUQ), left lower quadrant (LLQ), right upper quadrant (RUQ), and right lower quadrant (RLQ). Three scenarios for normal events have been considered:

1. Considering only the LUQ in Table 5, eight normal cases are generated in each row by controlling states of the breakers S_1, S_2, S_3, and S_4, which results in a total of 32 normal events ($2^{n-1} \times n$). In each simulated event of the 32 cases, states of the breakers, as shown in the RUQ of Table 5 (S_5, S_6, S_7, and S_8), are determined randomly by MCS. In order to determine the state of each breaker in the RUQ, a random number, uniformly distributed, is generated for each case, and rounded to the nearest

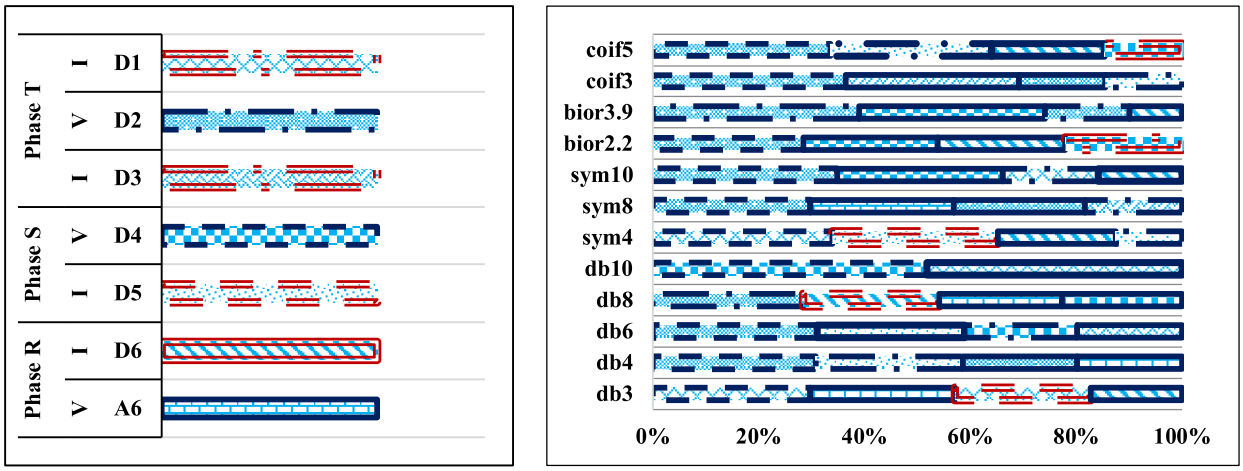

FIGURE 8. Features selected from the original signals using the MRMR algorithm. (a) Features' description. (b) Features selected by the corresponding wavelet function.

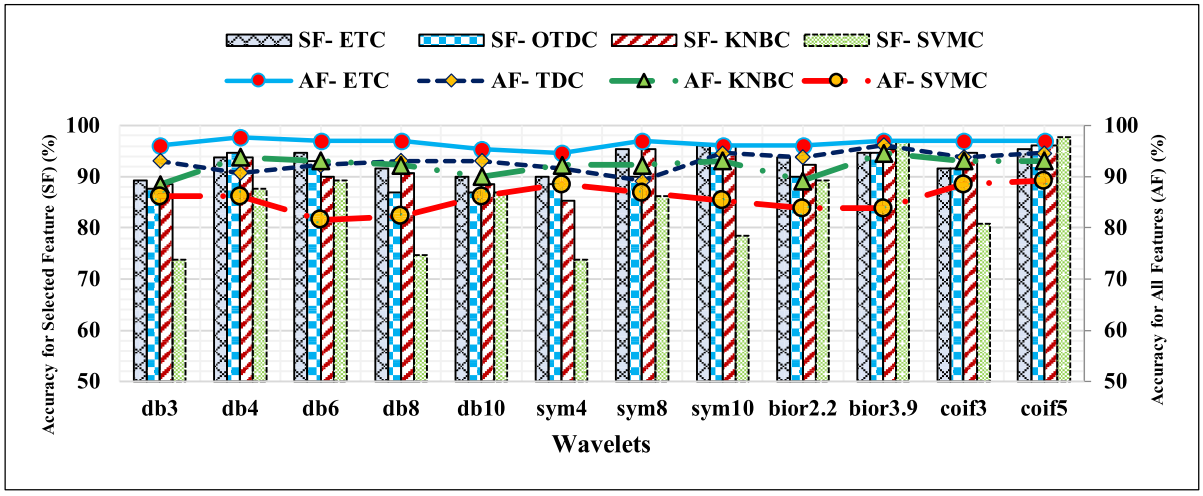

FIGURE 9. Classification accuracies as a percentage, using all features and selected features of the original signals.

integer (i.e., 0 or 1) where 0 indicates that the breaker is open and 1 means that the breaker is closed.

2. Considering the RLQ in Table 5, by controlling the states of the breakers S_5, S_6, S_7, and S_8, eight normal events are generated. Contrary to the normal events generated in the previous point, one breaker always switches off at time $t = 1.5\ s$, as shown in the RLQ of Table 5, resulting in a total of 32 normal events. In each simulated event of the 32 cases, states of the breakers shown in the LLQ of Table 5 (S_1, S_2, S_3, and S_4) are assigned randomly by MCS, as previously indicated.
3. Considering the RUQ and LLQ of Table 5, for each simulated event in this case, the state of any breaker is determined randomly using a uniform distribution, as stated in point one, and activated at time $t = 0\ s$. Furthermore, PV irradiance and temperature are predicted randomly based on MCS and their values drawn uniformly from $[\Gamma_{min}, \Gamma_{max}]$ and $[\gamma_{min}, \gamma_{max}]$, respectively. Here Γ_{min} and Γ_{max} are the lower and upper bounds of the PV irradiance values (i.e., 500 and 1750) and γ_{min} and γ_{max} are the minimum and maximum PV temperature values (i.e., 4 and 55). For each simulated event, the value of PV irradiance and temperature are assigned at time $t = 0\ s$, and at time $t = 1.5\ s$, a disturbance value, Γ_{dis} and γ_{dis}, is added/subtracted to/from the random assigned value (i.e., 150 and 7) in order to mimic a weather disturbance at that instance of time. A total of 64 cases (8^2) are simulated and labeled as normal events, implying that eight disturbance values are utilized per parameter considered in this scenario. It is worth noting that the normal events are simulated in the first two scenarios, given that the PV irradiance and temperature are Γ_r and γ_r.

2) SEMULATED ANOMALY EVENTS

Fault events are simulated in batches where each batch has three fault parameters, namely: fault type, fault resistance, and fault location. The first two parameters are determined as explained in point (2) of Section IV-C. However, fault

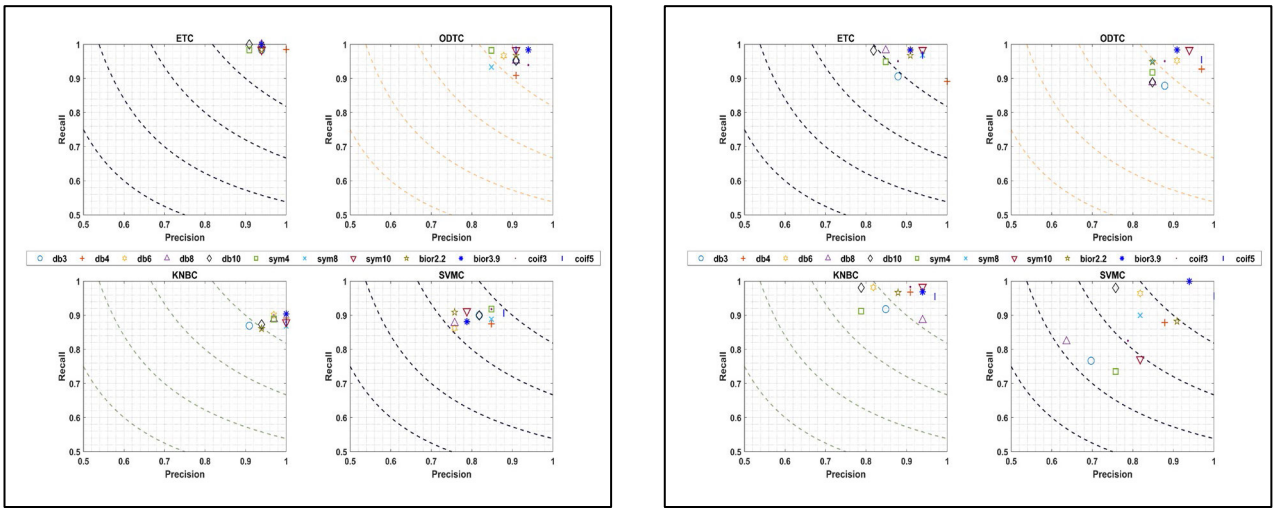

FIGURE 10. Results of precision and recall for different classifiers using the original signals. (a) Results using all features. (b) Results using selected features as per the MRMR algorithm.

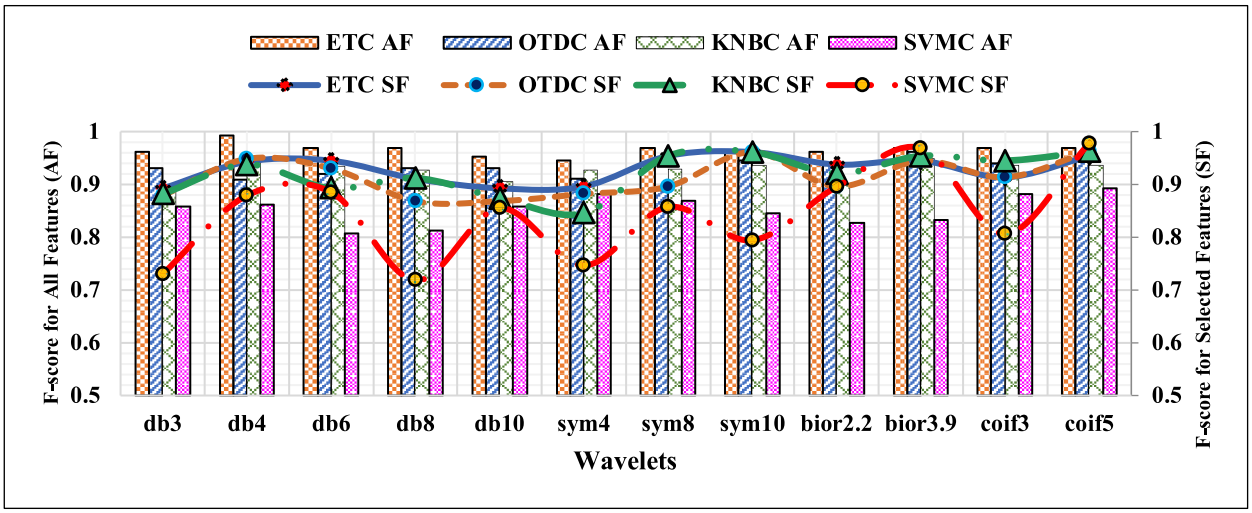

FIGURE 11. F-score results using all features and selected features of the original signals.

location is assigned randomly using MCS by generating a random integer number uniformly distributed over the interval of $[\tau_{min}, \tau_{max}]$, where τ_{min} and τ_{max} are the minimum and maximum distances as a percentage of the total line length. A total of 66 events have been simulated per batch and two batches of faults have been considered.

E. EVALUATION OF CASE 2

In this case study, the three-phase current and voltage samples measured at the PCC are used to build the attribute matrix. The attribute matrix is decomposed by the DWT and fed to machine learning classifiers, as explained in Section III-D and Section III-F, respectively. The evaluation in this case relies on two different methods, the first of which utilizes the original current and voltage signals as monitored at the PCC where the second method of assessment uses the difference between two samples, one cycle apart, of the current and voltage signals as measured at the PCC. In each method, four classifiers (ODTC, ETC, KNBC, and SVMC) are trained, by 50 % of the normal and anomaly events (160 cases), and tested by the other 50% cases, using two approaches: 1) all features as extracted by the DWT; and 2) selected features as explained in Section III-E.

1) PERFORMANCE EVALUATION BASED ON ORIGINAL CURRENT AND VOLTAGE SIGNALS

Features that were selected by each wavelet function from the original waveforms are displayed in Fig. 8(b), where their importance as a percentage is shown in the x-axis, and can be described based on the phase number (i.e., R, S, or T).

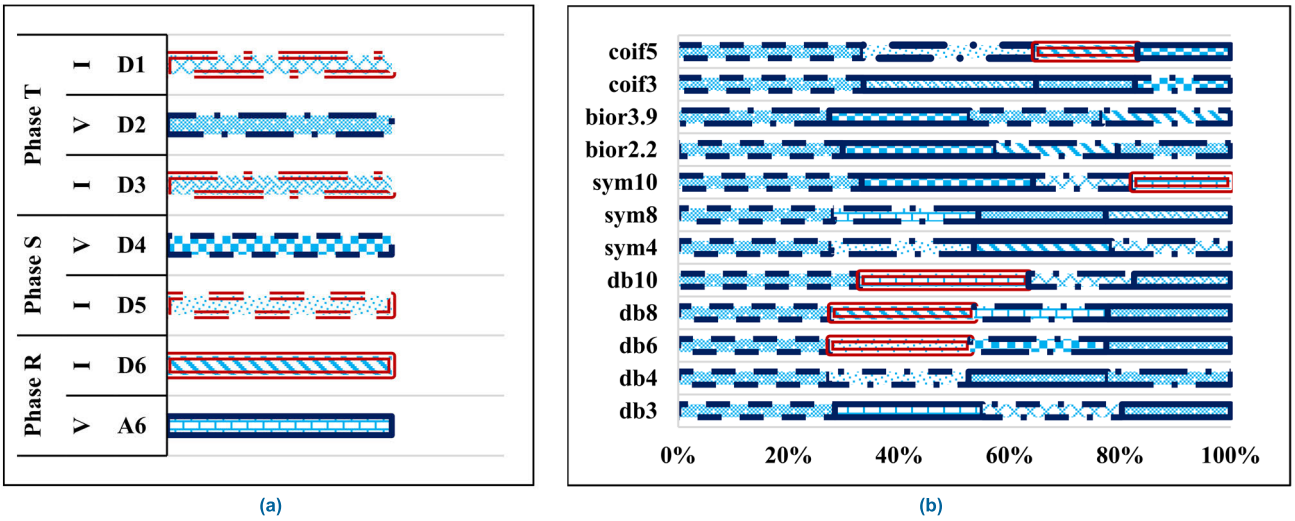

FIGURE 12. Features selected using the MRMR algorithm for the case when the change between samples is utilized. (a) Features' description. (b) Features selected by the corresponding wavelet function.

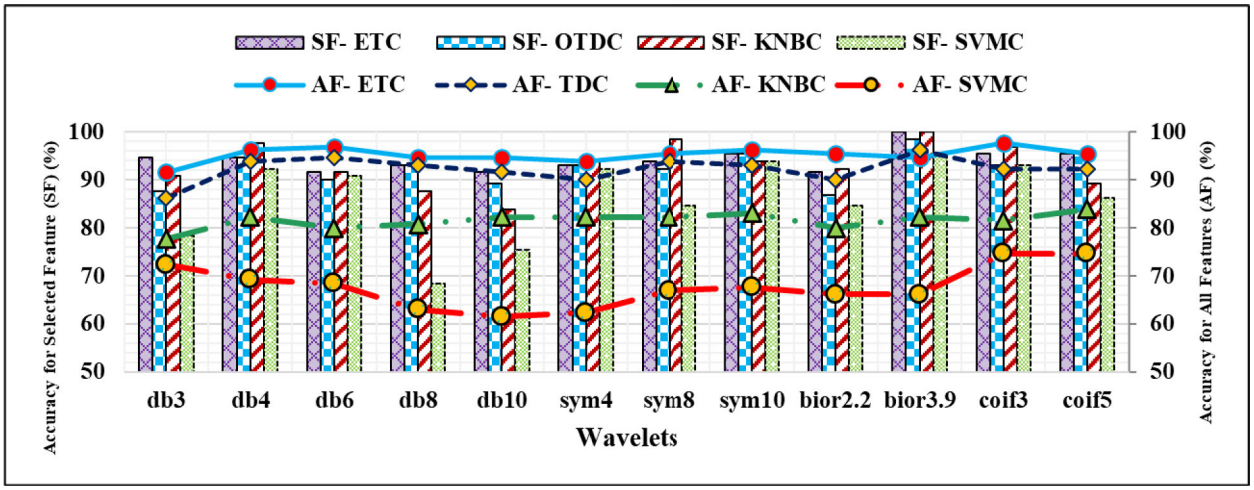

FIGURE 13. Classification accuracies as a percentage when the change between samples is utilized using all features and selected features.

The signal, whether current or voltage (i.e., I or V), and the wavelet level of decomposition (i.e., A6, D6, …, D1), are presented in Fig. 8(a). Fig. 9 presents the classification accuracies of each classifier tested by using all the features (AF) and some of the features (SF) selected from the original current and voltage values.

The results show that when all the features (42 features) are used, the performance of the classifiers is improved, especially for ETC. As an example, when Daubechies of order 4 (db 4) is trained by ETC and used to classify events into normal and anomaly, it provides 97.7% classification accuracy. The precision and recall are calculated and illustrated in Fig. 10. These two metrics are a commonly utilized tool when there is imbalance in the dataset. Inspection of Fig. 10(a) shows that biorthogonal of order 3.9 (bior3.9) achieves 1 per unit, for the precision and for the recall, when ETC and KNBC are utilized to train and test the decomposed original signals using all features, respectively. Hence, ETC is able to accurately classify all events that belong to the true negative class (normal events) when bior3.9 is utilized. However, some data of the true positive class (abnormal events) are misclassified as normal events as the precision values for ETC indicate (< 1 p.u.). In contrast, this means that KNBC is able to accurately classify all events that belong to the true positive class (abnormal events) when bior3.9 is utilized, but some data belonging to the true negative class (normal events) are misclassified as abnormal events as the recall values for KNBC indicate (< 1 p.u.). Moreover, Fig. 10 indicates that, using the selected features shown in Fig. 8(b), SVMC is able to accurately classify all events that belong to the true negative class (normal events) when bior3.9 is utilized. Based on the values of precision and recall, the

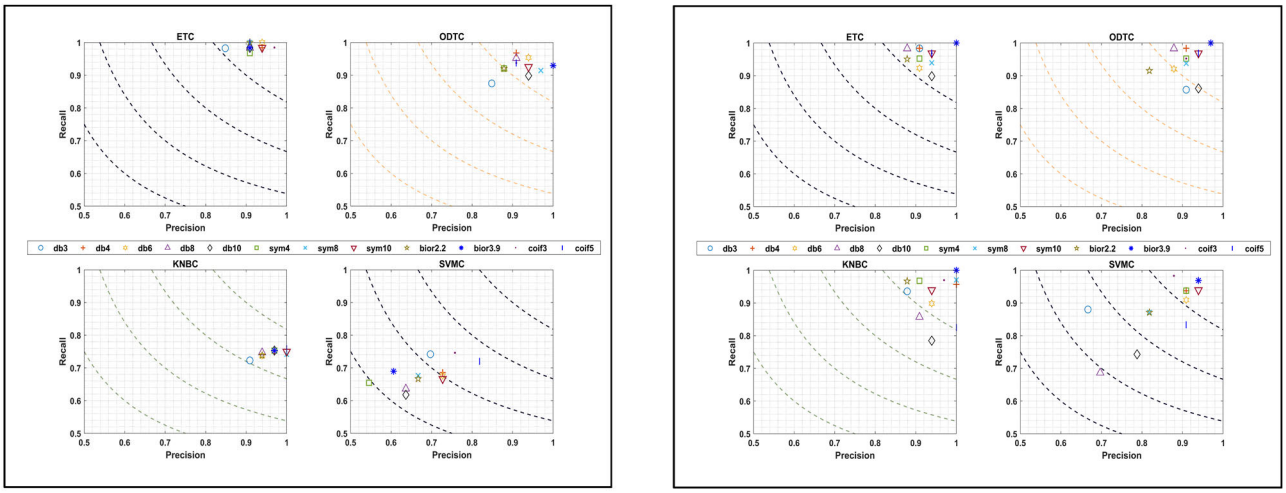

FIGURE 14. Results of precision and recall for different classifiers using the change between samples. (a) Results using all features. (b) Results using selected features as per the MRMR algorithm.

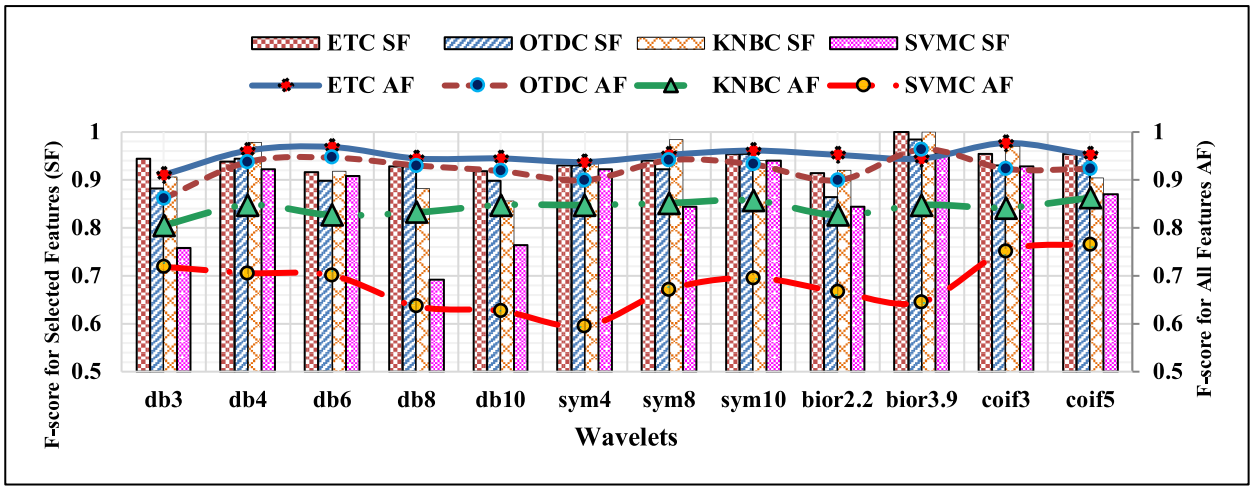

FIGURE 15. F-score results using all features and selected features while considering the change between samples.

values of the F-score are calculated as depicted in Fig. 11, where the results indicated by the F-score show that training and testing the ETC by all the features extracted using db4 from the original signals achieves the highest F-score, which is more than 0.99.

2) PERFORMANCE EVALUATION BASED ON THE DIFFERENCE OF SAMPLES OF CURRENT AND VOLTAGE SIGNALS

In this case, the difference of each consecutive sample of the current and voltage waveforms is utilized to collect the data set. The classifiers are assessed based on all features extracted by wavelet functions, as well as some of the features presented in Fig. 12(b), and extracted as illustrated in Section III-E. The performance results of testing all classifiers using the classification accuracies are displayed in Fig. 13. Inspection of Fig. 13 reveals that the obtained classification accuracies using bior3.9 are 100% when ETC and KNBC are trained and tested by the selected features shown in Fig. 12(b). This means that, instead of using the original signal, using the difference of each consecutive sample exhibits the hidden features leading to improved classifier performance. The results of precision and recall, which are presented in Fig. 14, indicate that performance of the classifiers is superior when these classifiers use only selected features compared to using all of them. When the features are selected as depicted in Fig. 12(b), for example, ETC and KNBC are able to accurately classify all normal and anomaly events with their corresponding classes. Both classifiers achieve precision and recall of 1, as shown in Fig.14(b), demonstrating a significant improvement in performance. The results of the F-score, which are presented in Fig. 15,

show that biorthogonal of order 3.9 (bior3.9) outperforms the other wavelet functions such as Daubechies, Coiflets, and Symlets. Furthermore, when bior3.9 is trained and tested by the selected features, using either ETC or KNBC, the F-score is 1, meaning that all data of true negative class are classified correctly as well as indicating that none of the data belonging to the true positive class is misclassified.

F. DISCUSSION

In this paper, four classifiers (ETC, SVMC, OTDC, and KNBC) are proposed as a means to detecting the origin of voltage sag, whether caused by a fault in the distribution power system (anomaly events) or because of a charging event occurring at a fast charging station (normal events). Two methods are utilized to train and test the classifiers: using the original current and voltage signals; and using the difference of each consecutive sample of their signals. Different wavelet families of different orders are utilized to decompose the signals from each utilized method. The evaluation results show that considering the difference of each consecutive sample leads to improved performance of the classifiers. Furthermore, the findings highlight the importance of the selected features as well as the wavelet function in accurately detecting anomalies in the power system. Biorthogonal of order 3.9 (bior3.9) is the best wavelet function that can be used in detecting and classifying the origin of voltage sags in a distribution network, if the relevant features have been selected and trained using either an ensemble tree classifier or a kernel naïve Bayes classifier.

V. CONCLUSION

In this paper, the impact of a fast charging station on voltage sag is quantified using two indices, as recommended by IEEE Std 1564-2014: the voltage sag energy index and the voltage sag severity index. The origin of voltage sag events is also determined as due either to a fault in the system or to a charging event that occurs at an FCS. Therefore, a machine learning-based method is proposed to accurately classify the origin of voltage sag as normal or anomaly events. Normal events are represented by charging events that occurred at the fast chargers, whether individually or as a combination. Anomaly events are represented by applying different fault scenarios that rely on various fault resistance and locations. The cases of both normal and anomaly events are generated based on a Monte Carlo simulation. Different wavelet functions of different orders are introduced to extract events' features relying on the change between cycles of the voltage and the current waveform. The minimum redundancy maximum relevance algorithm is applied in order to obtain an optimal set of features to improve the classification's performance. The results of classification of all normal and abnormal events reveal that the obtained classification accuracies using biorthogonal of order 3.9 are 100%, when ensemble tree or naïve Bayes classifiers are trained and tested by the selected optimal features. This research provides a helpful tool for power system operators who seek to improve the grid's reliability and stability.

ACKNOWLEDGMENT

The author extends his appreciation to the Deputyship for Research & Innovation, Ministry of Education in Saudi Arabia for funding this research work through the project number 223202.

REFERENCES

[1] J. C. Gomez and M. M. Morcos, "Voltage sag and recovery time in repetitive events," *IEEE Trans. Power Del.*, vol. 17, no. 4, pp. 1037–1043, Oct. 2002.

[2] C. J. Melhorn, T. D. Davis, and G. E. Beam, "Voltage sags: Their impact on the utility and industrial customers," *IEEE Trans. Ind. Appl.*, vol. 34, no. 3, pp. 549–558, Feb. 1998.

[3] M. H. J. Bollen, "Voltage sags: Effects, mitigation and prediction," *Power Eng. J.*, vol. 10, no. 3, pp. 129–135, Jun. 1996.

[4] Y. Wang, S. Li, and X.-Y. Xiao, "Estimation method of voltage sag frequency considering transformer energization," *IEEE Trans. Power Del.*, vol. 36, no. 6, pp. 3404–3413, Dec. 2021.

[5] G. Lv, C. Chu, Y. Zang, and G. Chen, "Voltage sag source location estimation based on optimized configuration of monitoring points," *CPSS Trans. Power Electron. Appl.*, vol. 6, no. 3, pp. 242–250, Sep. 2021.

[6] A. Khergade, R. Satputaley, and S. K. Patro, "Investigation of voltage sags effects on ASD and mitigation using ESRF theory-based DVR," *IEEE Trans. Power Del.*, vol. 36, no. 6, pp. 3752–3764, Dec. 2021.

[7] C. Tu, Q. Guo, F. Jiang, C. Chen, X. Li, F. Xiao, and J. Gao, "Dynamic voltage restorer with an improved strategy to voltage sag compensation and energy self-recovery," *CPSS Trans. Power Electron. Appl.*, vol. 4, no. 3, pp. 219–229, Sep. 2019.

[8] Y. Han, Y. Feng, P. Yang, L. Xu, Y. Xu, and F. Blaabjerg, "Cause, classification of voltage sag, and voltage sag emulators and applications: A comprehensive overview," *IEEE Access*, vol. 8, pp. 1922–1934, 2020.

[9] J. R. Camarillo-Peñaranda and G. Ramos, "Characterization of voltage sags due to faults in radial systems using three-phase voltage ellipse parameters," *IEEE Trans. Ind. Appl.*, vol. 54, no. 3, pp. 2032–2040, May 2018.

[10] M. N. Moschakis and N. D. Hatziargyriou, "Analytical calculation and stochastic assessment of voltage sags," *IEEE Trans. Power Del.*, vol. 21, no. 3, pp. 1727–1734, Jul. 2006.

[11] C.-H. Park, J.-H. Hong, and G. Jang, "Assessment of system voltage sag performance based on the concept of area of severity," *IET Gener., Transmiss. Distrib.*, vol. 4, no. 6, pp. 683–693, 2010.

[12] S. Arias-Guzmán, O. A. Ruiz-Guzmán, L. F. Garcia-Arías, M. Jaramillo-Gonzáles, P. D. Cardona-Orozco, A. J. Ustariz-Farfán, E. A. Cano-Plata, and A. F. Salazar-Jiménez, "Analysis of voltage sag severity case study in an industrial circuit," *IEEE Trans. Ind. Appl.*, vol. 53, no. 1, pp. 15–21, Jan. 2017.

[13] J. Lamoree, D. Mueller, P. Vinett, W. Jones, and M. Samotyj, "Voltage sag analysis case studies," *IEEE Trans. Ind. Appl.*, vol. 30, no. 4, pp. 1083–1089, Mar. 1994.

[14] M. H. J. Bollen, "Fast assessment methods for voltage sags in distribution systems," *IEEE Trans. Ind. Appl.*, vol. 32, no. 6, pp. 1414–1423, Jan. 1996.

[15] K. Ding, K. W. E. Cheng, X. D. Xue, B. P. Divakar, C. D. Xu, Y. B. Che, D. H. Wang, and P. Dong, "A novel detection method for voltage sags," in *Proc. 2nd Int. Conf. Power Electron. Syst. Appl.*, Nov. 2006, pp. 250–255.

[16] R. Naidoo and P. Pillay, "A new method of voltage sag and swell detection," *IEEE Trans. Power Del.*, vol. 22, no. 2, pp. 1056–1063, Apr. 2007.

[17] Ö. Gencer, S. Öztürk, and T. Erfidan, "A new approach to voltage sag detection based on wavelet transform," *Int. J. Electr. Power Energy Syst.*, vol. 32, no. 2, pp. 133–140, Feb. 2010.

[18] R. C. Leborgne and D. Karlsson, "Voltage sag source location based on voltage measurements only," *Elect. Power Quality Utilisation J.*, vol. 14, pp. 25–30, Jun. 2008.

[19] G. Shahgholian, Z. Azimi, and J. Faiz, "Voltage sag in distribution systems—A review and comparative study (reasons, characteristics, compensations and detection)," *J. Electr. Power Energy Convers. Syst.*, vol. 1, no. 3, pp. 107–119, 2016.

[20] P. Thakur, A. K. Singh, and R. C. Bansal, "Novel way for classification and type detection of voltage sag," *IET Gener., Transmiss. Distrib.*, vol. 7, no. 4, pp. 398–404, Apr. 2013.
[21] C. Becker, W. Braun, K. Carrick, T. Diliberti, C. Grigg, J. Groesch, B. Hazen, T. Imel, D. Koval, D. Mueller, T. S. John, and L. E. Conrad, "Proposed chapter 9 for predicting voltage sags (dips) in revision to IEEE Std 493, the gold book," *IEEE Trans. Ind. Appl.*, vol. 30, no. 3, pp. 805–821, Jun. 1994.
[22] M. R. Qader, M. H. J. Bollen, and R. N. Allan, "Stochastic prediction of voltage sags in a large transmission system," *IEEE Trans. Ind. Appl.*, vol. 35, no. 1, pp. 152–162, Jan. 1999.
[23] J. Y. Chan and J. V. Milanovic, "Assessment of the economic value of voltage sag mitigation devices to sensitive industrial plants," *IEEE Trans. Power Del.*, vol. 30, no. 6, pp. 2374–2382, Dec. 2015.
[24] J. V. Milanovic and C. P. Gupta, "Probabilistic assessment of financial losses due to interruptions and voltage sags—Part I: The methodology," *IEEE Trans. Power Del.*, vol. 21, no. 2, pp. 918–924, Apr. 2006.
[25] M. F. McGranaghan, D. R. Mueller, and M. J. Samotyj, "Voltage sags in industrial systems," *IEEE Trans. Ind. Appl.*, vol. 29, no. 2, pp. 397–403, Oct. 1993.
[26] C.-C. Shen and C.-N. Lu, "A voltage sag index considering compatibility between equipment and supply," *IEEE Trans. Power Del.*, vol. 22, no. 2, pp. 996–1002, Apr. 2007.
[27] C. P. Gupta and J. V. Milanovic, "Probabilistic assessment of equipment trips due to voltage sags," *IEEE Trans. Power Del.*, vol. 21, no. 2, pp. 711–718, Apr. 2006.
[28] E. C. Aeloiza, P. N. Enjeti, L. A. Moran, O. C. Montero-Hernandez, and S. Kim, "Analysis and design of a new voltage sag compensator for critical loads in electrical power distribution systems," *IEEE Trans. Ind. Appl.*, vol. 39, no. 4, pp. 1143–1150, Jul. 2003.
[29] P. Heine, P. Pohjanheimo, M. Lehtonen, and E. Lakervi, "A method for estimating the frequency and cost of voltage sags," *IEEE Trans. Power Syst.*, vol. 17, no. 2, pp. 290–296, May 2002.
[30] J. A. Martinez and J. Martin-Arnedo, "Voltage sag studies in distribution networks—Part II: Voltage sag assessment," *IEEE Trans. Power Del.*, vol. 21, no. 3, pp. 1679–1688, Jul. 2006.
[31] C.-H. Park and G. Jang, "Stochastic estimation of voltage sags in a large meshed network," *IEEE Trans. Power Del.*, vol. 22, no. 3, pp. 1655–1664, Jul. 2007.
[32] *IEEE Guide for Voltage Sag Indices*, IEEE Standard 1564-2014, 2014, doi: 10.1109/IEEESTD.2014.6842577.
[33] *Materials International (SEMI), Specification for Semiconductor Processing Equipment Voltage Sag Immunity*, Standard F47-0706, 2006.
[34] S. Wang and H. Chen, "A novel deep learning method for the classification of power quality disturbances using deep convolutional neural network," *Appl. Energy*, vol. 235, pp. 1126–1140, Feb. 2019.
[35] M. Mishra, "Power quality disturbance detection and classification using signal processing and soft computing techniques: A comprehensive review," *Int. Trans. Electr. Energy Syst.*, vol. 29, no. 8, Aug. 2019, e12008.
[36] P. S. Wright, "Short-time Fourier transforms and Wigner–Ville distributions applied to the calibration of power frequency harmonic analyzers," *IEEE Trans. Instrum. Meas.*, vol. 48, no. 2, pp. 475–478, Apr. 1999.
[37] S. Khokhar, A. A. Mohd Zin, A. P. Memon, and A. S. Mokhtar, "A new optimal feature selection algorithm for classification of power quality disturbances using discrete wavelet transform and probabilistic neural network," *Measurement*, vol. 95, pp. 246–259, Jan. 2017.
[38] R. Ahila, V. Sadasivam, and K. Manimala, "An integrated PSO for parameter determination and feature selection of ELM and its application in classification of power system disturbances," *Appl. Soft Comput.*, vol. 32, pp. 23–37, Jul. 2015.
[39] M. Biswal and P. K. Dash, "Detection and characterization of multiple power quality disturbances with a fast S-transform and decision tree based classifier," *Digit. Signal Process.*, vol. 23, no. 4, pp. 1071–1083, Jul. 2013.
[40] M. Sahani and P. K. Dash, "FPGA-based online power quality disturbances monitoring using reduced-sample HHT and class-specific weighted RVFLN," *IEEE Trans. Ind. Informat.*, vol. 15, no. 8, pp. 4614–4623, Aug. 2019.
[41] K. Thirumala, M. S. Prasad, T. Jain, and A. C. Umarikar, "Tunable-Q wavelet transform and dual multiclass SVM for online automatic detection of power quality disturbances," *IEEE Trans. Smart Grid*, vol. 9, no. 4, pp. 3018–3028, Jul. 2018.
[42] P. D. Achlerkar, S. R. Samantaray, and M. S. Manikandan, "Variational mode decomposition and decision tree based detection and classification of power quality disturbances in grid-connected distributed generation system," *IEEE Trans. Smart Grid*, vol. 9, no. 4, pp. 3122–3132, Jul. 2018.
[43] K. Chen, J. Hu, and J. He, "A framework for automatically extracting overvoltage features based on sparse autoencoder," *IEEE Trans. Smart Grid*, vol. 9, no. 2, pp. 594–604, Mar. 2018.
[44] W. H. Kersting, "Radial distribution test feeders," in *Proc. IEEE Power Eng. Soc. Winter Meeting, Conf.*, Feb. 2001, pp. 908–912, doi: 10.1109/PESW.2001.916993.
[45] *Resources—IEEE PES Test Feeder*. Accessed: Jul. 13, 2023. [Online]. Available: https://cmte.ieee.org/pes-testfeeders/resources/
[46] *Simple Solar Farm*. Accessed: Apr. 3, 2023. [Online]. Available: https://www.pscad.com/knowledge-base/article/521
[47] S. R. Mohanty, A. K. Pradhan, and A. Routray, "A cumulative sum-based fault detector for power system relaying application," *IEEE Trans. Power Del.*, vol. 23, no. 1, pp. 79–86, Jan. 2008.
[48] F. B. Costa and J. Driesen, "Assessment of voltage sag indices based on scaling and wavelet coefficient energy analysis," *IEEE Trans. Power Del.*, vol. 28, no. 1, pp. 336–346, Jan. 2013.
[49] F. B. Costa, B. A. Souza, and N. S. D. Brito, "Real-time detection of voltage sags based on wavelet transform," in *Proc. IEEE/PES Transmiss. Distrib. Conf. Expo., Latin Amer.*, Nov. 2010, pp. 537–542.
[50] M. B. Latran and A. Teke, "A novel wavelet transform based voltage sag/swell detection algorithm," *Int. J. Electr. Power Energy Syst.*, vol. 71, pp. 131–139, Oct. 2015.
[51] G. Zheng, X.-M. Yan, H.-W. Li, and D. Liu, "Classification of voltage sag based on wavelet transform and wavelet network," in *Proc. Int. Conf. Mach. Learn. Cybern.*, 2004, pp. 466–470.
[52] C. Ding and H. Peng, "Minimum redundancy feature selection from microarray gene expression data," *J. Bioinf. Comput. Biol.*, vol. 3, no. 2, pp. 185–205, Apr. 2005.
[53] P.-N. Tan, M. Steinbach, and V. Kumar, *Introduction to Data Mining*. London, U.K.: Pearson, 2016.
[54] T. G. Dietterich, "An experimental comparison of three methods for constructing ensembles of decision trees: Bagging, boosting, and randomization," *Mach. Learn.*, vol. 40, no. 2, pp. 139–157, Aug. 2000.
[55] Y. Murakami and K. Mizuguchi, "Applying the Naïve Bayes classifier with kernel density estimation to the prediction of protein–protein interaction sites," *Bioinformatics*, vol. 26, no. 15, pp. 1841–1848, Aug. 2010.
[56] A. Statnikov, *A Gentle Introduction to Support Vector Machines in Biomedicine: Theory and Methods*, vol. 1. Singapore: World Scientific, 2011.
[57] M. Sokolova, N. Japkowicz, and S. Szpakowicz, "Beyond accuracy, F-score and ROC: A family of discriminant measures for performance evaluation," in *Proc. Aust. Conf. Artif. Intell.*, 2006, pp. 1015–1021.

SAMI M. ALSHAREEF (Member, IEEE) received the B.Sc. (Eng.) degree in electrical engineering from Umm Al-Qura University, Mecca, Saudi Arabia, in 2009, and the M.Sc. (Eng.) and Ph.D. degrees in electrical engineering from Ontario Tech University (UOIT), Oshawa, Canada, in 2014 and 2020, respectively. He is currently an Assistant Professor with Jouf University, Sakaka, Saudi Arabia. His research interests include smart grid, transportation electrification, and cybersecurity.